EngOpt 2012 - International Conference on Engineering Optimization
Rio de Janeiro, Brazil, 1-5 July 2012.

Inverse parameter identification for a branching 1D arterial network

A.E.J. Bogaers[1], S. Kok[1], B.D. Reddy[2,3], T. Franz[3,4]

[1]Advanced Mathematical Modelling, MDS, CSIR, Pretoria, South Africa
[2]Department of Mathematics and Applied Mathematics, University of Cape Town, Rondebosch, South Africa
[3]Centre for Research in Computational and Applied Mechanics, University of Cape Town, Rondebosch, South Africa
[4]Cardiovascular Research Unit, Faculty of Health Sciences, Universtiy of Cape Town, Observatory, South Africa

Abstract

In this paper we investigate the invertability of a branching 1D arterial blood flow network. We limit our investigation to a single bifurcating vessel, where the material properties, unloaded areas and variables characterizing the input and output boundary conditions are included as free parameters. The synthetic time data used for the optimization problem, as well as the blood flow analysis is performed using a 1D finite volume vascular network model. We pose and investigate four different problem formulations based on synthetic data which could hypothetically be measured experimentally. We will demonstrate the invertibality of the problem based on synthetic time data at a single location within the bifurcation as well as demonstrate the influance of the number of data points included within these time signals. Lastly, we will show how the addition of increasing levels of noise to the synthetic data influences the ability of obtaining the correct system parameters. For purposes of the inverse optimization we make use of a bounded BFGS algorithm where the gradients are approximated using the complex step method.

Keywords: Inverse parameter identification, 1D branching blood flow, complex step method.

1 Introduction

Mathematical and numerical modelling of the cardiovascular system has received considerable attention in recent years. In this context, simplified models, including 1 dimensional models have demonstrated potential in providing useful information and insight pertaining to the global flow through the vascular network at computationally reasonable times. To illustrate typical results achievable with a 1D model consider Figure 1, which depicts the pressure pulse propagation through the ascending aorta, left femoral artery and left tibial artery. The pressure pulses are generated using a 1 dimensional finite volume model [1] for blood flow through a 55 artery network model.

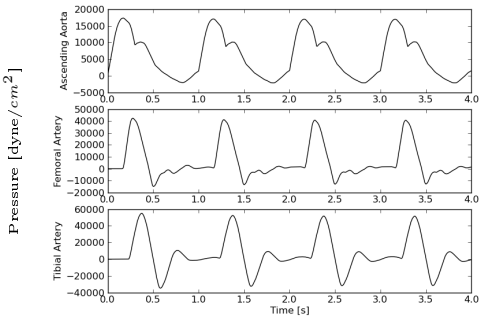

Figure 1: Pressure pulse profiles for blood flow through a 55 vascular network model computed using a 1D finite volume blood flow model [1].

Such a model could indeed be useful to medical practitioners, provided that the model can be characterised to produce physiologically realistic flows for the unique pathology of a given patient. The

model can be used by surgeons to obtain insight into the effect of planned surgery, for example the global effect on blood flow when inserting a vascular graft, or choosing the size of an arterial-venous shunt to be inserted for purposes of haemodialysis treatment. It could further be used to assist in ascertaining post-operative success of various surgeries or be used to provide patient specific boundary conditions for a higher fidelity 3 dimensional fluid structure interactions (FSI) model for a given area of interest.

This does however require that such a model be capable of being characterised to the unique vascular pathology of a given patient. Several studies to date have demonstrated the invertibility of a 1 dimensional model to determine the material properties of a single artery. The studies have predominantly focused on using synthetic data obtained using a full 3D FSI simulation for an artery with a single homogeneous material property [3] as well as for arteries with non-uniform properties due to the presence of abnormalities such as aneurysms [2].

It is possible, through both invasive and non-invasive techniques to obtain time data at one or more locations of either pressure, volume flow rate or area for flow through the vascular system. This can be done through invasive pressure probes inserted into an artery or non-invasive imaging techniques such as MRI or ultra-sound scans. In this paper we aim to investigate the invertibility of a branching 1D vascular network using data of this nature.

The analysis is performed using a 1D finite volume (FV) code implemented on a staggered grid to solve the one dimensional area-velocity continuity equations. The model has been demonstrated to accurately capture the various reflecting pressure waves for a network with arbitrary discontinuities in compliance as well as branching vessels.

2 1D Blood Flow Model

2.1 Governing Equations

The mass and momentum equations for a cylindrical vessel with compliant walls expressed in terms of area and velocity can be shown to be [5, 6]:

$$\frac{\partial A}{\partial t} + \frac{\partial (Au)}{\partial x} = 0 \tag{1}$$

$$\frac{\partial u}{\partial t} + u\frac{\partial u}{\partial x} + \frac{1}{\rho}\frac{\partial p}{\partial x} + K_R\frac{u}{A} = 0 \tag{2}$$

where A, p and u are cross-sectional luminal area of the vessel, fluid pressure and velocity respectively. K_R is a function representing viscous losses. Assuming fully developed steady flow with a flat velocity profile the viscous losses can be approximated by

$$K_R\frac{u}{A} = -\frac{8\pi\mu u}{A}, \tag{3}$$

where μ is the blood viscosity.

The mass (1) and momentum (2) equations however have 3 unknowns. To close the set of equations, an algebraic area-pressure relationship is used which is of the form:

$$p = p_{\text{ext}} + \phi\left(A, A_0, \beta\right) \tag{4}$$

where p_{ext} represents external pressure, A_0 is the initial unloaded area (artery area when $p_{\text{ext}} = 0$) and β is a function describing material properties. In this paper we use a non-linear pressure-area relationship of the form [5]

$$p = p_{\text{ext}} + \beta\left(\sqrt{A} - \sqrt{A_0}\right), \tag{5}$$

where β is defined as

$$\beta = \frac{\sqrt{\pi}hE}{A_0\left(1-\sigma^2\right)}, \tag{6}$$

and h is the artery thickness, E is Young's modulus and σ is Poisson's ratio.

2.2 Numerical Discretization

In this paper, equations (1) and (2) are solved using the FV method on a staggered grid (see Figure 2). This allows for as many equations as there are unknowns, and hence no additional compatibility equations are required.

Firstly, the mass and momentum conservation equations are modified to be in terms of the quantities to be conserved, i.e. volume flow rate $Q = Au$ and total pressure $p_0 = \frac{1}{2}\rho u^2 + p$.

To this end, the mass (1) and momentum (2) equations become

$$\frac{\partial A}{\partial t} + \frac{\partial Q}{\partial x} = 0, \tag{7}$$

$$\rho \frac{\partial}{\partial t}\left(\frac{Q}{A}\right) + \frac{\partial p_0}{\partial x} + K_R \frac{Q}{A^2} = 0, \tag{8}$$

where

$$p_0 = p_{\text{ext}} + \beta\left(\sqrt{A} - \sqrt{A_0}\right) + \frac{1}{2}\rho\left(\frac{Q}{A}\right)^2. \tag{9}$$

Consider Figure 2(a). There are two sets of control volumes (CVs). Areas and pressures are associated with the one set of CVs, indicated by subscript i, and momentum conservation is associated with the other set of CVs indicated with subscript I. The midpoint of each of the groups is defined such that their quantities are at the face centres of the second group.

Assuming a uniform finite difference mesh (all $\Delta x_I = \Delta x_i = \Delta x$) the FV discretization of the mass and momentum equations for a generalised integral in time become:

$$\frac{A_i - A_i^0}{\Delta t}\Delta x = -\theta\left(Q_I - Q_{I-1}\right) - (1-\theta)\left(Q_I - Q_{I-1}\right)^0, \tag{10}$$

$$\left[\left(\frac{Q_I}{A_I}\right) - \left(\frac{Q_I}{A_I}\right)^0\right]\frac{\rho\Delta x}{\Delta t} = - \theta\left(\left(p_0^{i+1} - p_o^i\right) + K_R\frac{Q_I}{A_I^2}\Delta x\right) - (1-\theta)\left(\left(p_0^{i+1} - p_o^i\right) + K_R\frac{Q_I}{A_I^2}\Delta x\right)^0, \tag{11}$$

where the superscript '0' refers to the previous time step t and no superscript refers to time step $t + \Delta t$. Furthermore, integration in time is first order explicit if $\theta = 0$, second order Crank-Nicholson for $\theta = 1/2$ and first order implicit for $\theta = 1$. The area at the centre of the momentum CV is defined as $A_I = \frac{A_{i+1}+A_i}{2}$ and the discretised total pressure is

$$p_0^i = p_{\text{ext}}^i + \beta^i\left(\sqrt{A_i} - \sqrt{A_0^i}\right) + \frac{1}{2}\rho\left(\frac{Q_i}{A_i}\right)^2, \tag{12}$$

where $Q_i = \frac{Q_I + Q_{I-1}}{2}$.

Discretisation at branching vessels: For a branching vessel we use a staggered grid shown in Figure 2(b), where area and pressure node values are located at the centre of the branching CV. With this grid discretisation, both the momentum and mass conservation equations are naturally treated.

The mass and momentum discretised equations for the mesh in Figure 2(b) (for a uniform finite difference mesh where $\Delta x_i = \Delta x_I = \Delta x$) at the branching point become:

$$\frac{A_2 - A_2^0}{\Delta t}\left(\frac{3}{2}\Delta x\right) = -\theta\left(Q_3 + Q_2 - Q_1\right) - (1-\theta)\left(Q_3 + Q_2 - Q_1\right)^0 \tag{13}$$

$$\frac{\rho}{A_{2-4}}\frac{Q_3 - Q_3^0}{\Delta t}\Delta x = -\theta\left[\left(p_{0_4} - p_{0_2}\right) + K_R\frac{Q_3}{A_{2-4}^2}\Delta x\right] - (1-\theta)\left[\left(p_{0_4} - p_{0_2}\right) + K_R\frac{Q_3}{A_{2-4}^2}\Delta x\right]^0. \tag{14}$$

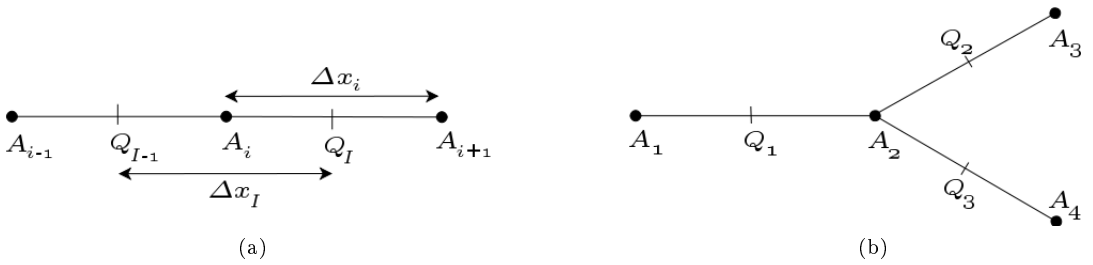

Figure 2: Staggered grid discretisation with associated control volumes for (a) linear vessel and (b) branching bifurcation.

The discretised total pressure equation becomes

$$p_{0_2} = p_{ext_2} + \beta_2 \left(\sqrt{A_2} - \sqrt{A_{0_2}} \right) + \frac{1}{2} \rho \left(\frac{Q_{2i}}{A_2} \right)^2 . \tag{15}$$

In order to compute Q_{2i} at the bifurcation, we make the assumption that $Q_1 = Q_2 + Q_3$ (i.e. values of Q at cell centres $= Q$ at face centres). Based on this assumption, volume flow rate at the bifurcation can be approximated as $Q_{2i} = \frac{1}{2} \left[(Q_1) + (Q_2 + Q_3) \right]$. It should be noted that when generating the mesh, the area and material properties at the bifurcation are interpolated to be consistent with this choice of Q interpolation.

3 Problem Formulation

3.1 Problem Description

In this paper, we will limit our discussion to the analysis of a single bifurcating vessel, as depicted in Figure 3. We will demonstrate that a single bifurcation is sufficiently complex to warrant analysis, while many of the conclusions drawn can be extrapolated to a larger network.

In order to uniquely define the bifurcating artery would require knowing the material property β, initial unloaded area A_0 and length L of each of the three arterial segments. It would further be necessary to characterise both the input and each of the respective outputs along with blood flow properties including density ρ and viscosity μ.

In this paper we will make the following simplifying assumptions. We will assume $\mu = 0$, such that there are no frictional losses, density will be fixed at $\rho = 1 g/\text{cm}^3$ while it will further be assumed that each of the artery lengths are known.

The input pulse is modelled as a half sine wave of the form:

$$\begin{aligned} p_{\text{in}} &= K \sin\left(\frac{2\pi t}{T} \right), \quad t \leq \frac{T}{2} \\ p_{\text{in}} &= 0, \quad t > \frac{T}{2} \end{aligned} \tag{16}$$

where K and T are the input wave amplitude and period respectively.

The artery outlets are modelled using a resistance coefficient such that $R_t = 0$ for non-reflecting outlet boundary conditions and conversely $R_t = 1$ for a fully reflecting outlet condition. The resistance coefficient is applied as demonstrated in [5] using the system characteristics.

3.2 Problem formulation and cost function

To demonstrate the ill-posed nature of the problem consider the three sets of material properties defined in Table 1. The pressure vs. time plot at the centre of vessel A for the three bifurcations are shown

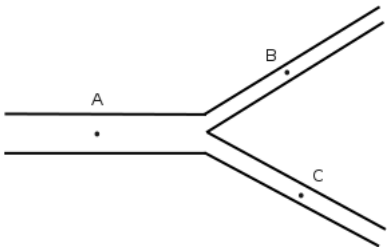

Figure 3: Depiction of bifurcating vessel.

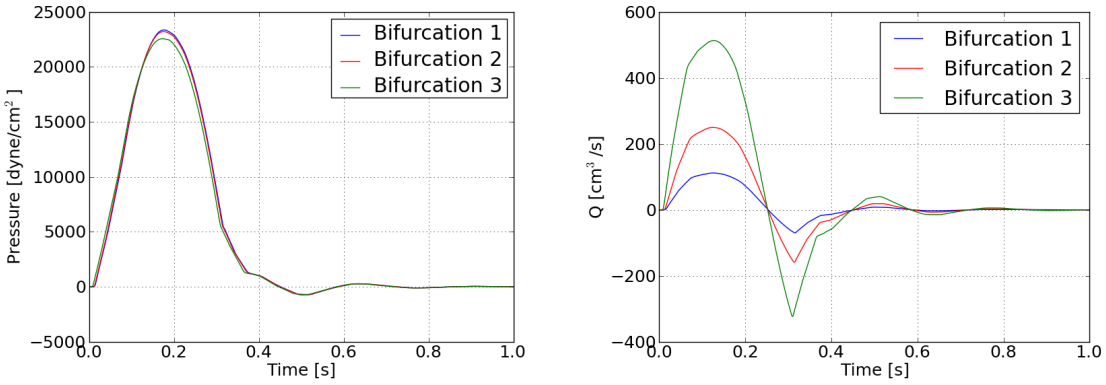

(a) (b)

Figure 4: Synthetic data at the centre of vessel A computed using the 1D FV solver for the material properties presented in Table 1 depicting (a) pressure-time data, where despite the large differences in material properties, the variation in the pressure-time data is minimal and (b) the volume flow rate which is distinct for the three sets of bifurcation properties.

in Figure 4(a). Despite the material properties in many instances varying close to 500%, the resulting pressure pulses vary only slightly, well within reasonable bounds of measurement error.

Table 1: Vessel properties for the bifurcating artery and the parameters to characterise the inlet and outlet boundary conditions used to generate the synthetic time data presented in Figure 4.

	β_A (dyne/cm^3)	β_B (dyne/cm^3)	β_C (dyne/cm^3)	A_{0_A} (cm^2)	A_{0_B} (cm^2)	A_{0_C} (cm^2)	R_{t_B}	R_{t_C}	K (dyne/cm^2)	T (s)
Bifurcation 1	113487	226974	453948	4.0	0.5	3.5	0.5	0.5	15×10^4	0.3
Bifurcation 2	85750.2	148762.8	269660.2	10.0	1.14	7.94	0.5	0.52	15×10^4	0.3
Bifurcation 3	100000	99091.6	136406	30	2.42	17	0.5	0.57	15×10^4	0.3

$L_A = 10cm$, $L_B = 20cm$, $L_C = 10cm$

There are several well known techniques to treat mathematically ill-posed problems. The most popular of these techniques is known as regularisation, whereby the inverse solution is mildly biased towards a set of assumed reasonable values for the given design variables. Regularisation does however heavily depend on having some understanding of what the solution should be prior to commencing the inverse analysis. This is somewhat problematic when considering the vascular network. For example, there is still no agreed upon range for arterial material properties β. This is partially due to the lack of in-vivo experimental measurements as well as the large variation from one individual to another. Furthermore, material properties can easily differ by several orders of magnitude as a result of diseased arteries, naturally occurring anomalies or even as a result of surgical intervention in the form of grafts.

For this reason we have opted to investigate the possibility of enriching the pressutre-time data with

additional non-related information. In this paper we will investigate 4 options, where hypothetically each option can be implemented based on existing medical data capturing devices.

Option 1: Pressure-time data only. As a first step, we will analyse the invertibility of the bifurcating vessel as a function of the pressure-time data only. The cost function to be minimised is defined as:

$$F_1(DV) = \sum_{i=0}^{N} \left(p(t_i) - p_{\text{given}}(t_i)\right)^2 \tag{17}$$

where N is the total number of data points within the pressure-time data and the design variables are $DV = [\beta_A, \beta_B, \beta_C, A_{0_A}, A_{0_B}, A_{0_C}, R_{t_B}, R_{t_C}, K, T]$.

Option 2: Including volume flow rate information. While the problem is ill-posed when considering only pressure-time data, it is possible to augment the information by including further information such as the volume flow rate, Q, at the same point. To illustrate this consider Figure 4(b) which depicts Q at the same measurement location for the three bifurcations. The additional information related to the 3 bifurcations are now distinct.

This cost function is defined as:

$$F_2(DV) = \sum_{i=0}^{N} \left[\frac{1}{10^4} \left(p(t_i) - p_{\text{given}}(t_i)\right)^2 + \left(Q(t_i) - Q_{\text{given}}(t_i)\right)^2 \right] \tag{18}$$

where the pressure data is divided by 10^4 to provide similar weight to both sets of data. $DV = [\beta_A, \beta_B, \beta_C, A_{0_A}, A_{0_B}, A_{0_C}, R_{t_B}, R_{t_C}, K, T]$.

Option 3: Fixing a single A_0 value. Since the flow through the vascular problem is predominantly a ratio based problem, the simplest means by which to render the problem well posed is to fix a single unknown area A_0 or material property β. In so doing, the remaining unknown variables can be obtained as a function relating to the single known quantity. For the purposes of this paper we assume that the unstressed area of vessel A (A_{0_A}) is known where the cost function is thus based only on the pressure-time data with A_{0_A} removed from the list of design variables:

$$F_3(DV_3) = \sum_{i=0}^{N} \left(p(t_i) - p_{\text{given}}(t_i)\right)^2 \tag{19}$$

for $DV_3 = [\beta_A, \beta_B, \beta_C, A_{0_B}, A_{0_C}, R_{t_B}, R_{t_C}, K, T]$.

Option 4: Including travel time between two points. The final option investigated for rendering the problem well posed is to include the travel time of the pressure pulse between two points in the branching network. This can be done by using two measuring devices placed at two locations along the vascular tree to record the instances in time when the pressure pulse propagates past the particular points of measurement.

We therefore assume we know the travel time between the centre of vessel A to the centre of vessel B and can hence formulate a function relating the difference between the computed time and the measured time such that

$$E = \left(\Delta\text{time}_{\text{computed}} - \Delta\text{time}_{\text{given}}\right)^2$$

where the cost function can then be defined as

$$F_4(DV) = \sum_{i=0}^{N} \log\left(\left(p(t_i) - p_{\text{given}}(t_i)\right)^2\right) + 10E. \tag{20}$$

It should be noted that the two contributions to the cost function are normalised such that their respective contributions are of similar order of magnitude.

It should further be noted that including a travel time as an additional constraint may cause the problem to remain ill-posed and result in a multi-modal functional space, especially if the measurement points extend over several different arterial vessels. This is because there are several possible combinations of artery pressure pulse speeds over a range of connecting vessels that can result in the same travel time. It thus remains important to have reasonable bounds to the inverse problem or have several such time measurement points.

3.3 Complex step gradients

The inverse optimisation problem is solved here using a limited-memory BFGS algorithm with bounded constraints [7]. It therefore is important to have available accurate and reliable gradients of the cost function with regards to the design variables. There are several means by which to obtain problem sensitivities, and often of concern are their respective accuracies, computational expense and ease of implementation. When considering optimisation problems involving a single cost function with several design variables, analytic or semi-analytic methods, whether the gradients are computed directly or via the adjoint method is often the preferred means when considering both expense and accuracy. It is however difficult to justify the additional effort required in obtaining these gradients while still in the early stages of solving an optimisation problem when issues such as problem formulation, cost function and choice of design variables are still uncertain and likely to change often.

Finite differences have gained popularity in this regards, primarily for the ease of implementation despite not being either particularly accurate, reliable or computationally efficient. For this reason we make use of the complex step method [4]. The method is arguably as easy to implement as finite differencing, but provides analytical or near analytical approximations to the function gradients.

Consider a simple forward differencing approximation:

$$f'(x) = \frac{f(x+h) - f(x)}{h} + \mathcal{O}(h), \tag{21}$$

where h is the step size. Via Taylor series expansion it can be shown that the error is $\mathcal{O}(h)$ and hence the approximation is first order accurate. It is desirable to use as small a step size as possible to minimise the truncation error. However, this often leads to inaccuracies due to differencing errors.

Using the complex step method, the gradient is approximated as:

$$f'(x) = \frac{\mathrm{Im}\left(f(x) + ih\right)}{h} + \mathcal{O}(h^2), \tag{22}$$

where the gradient is approximated as the imaginary part of a complex perturbation of the function divided by the real magnitude of the perturbation size. Taylor series expansion in the complex space shows that the error of the real solution is $\mathcal{O}(h^2)$ [4]. However, since there are no possible differencing errors one can use arbitrarily small perturbations. The complex step method does however require that the solver generating the function values be capable of treating complex numbers. Often this only requires modifying variable declarations from real to complex.

To illustrate the accuracy of the complex step method, consider the results in Table 2. In the table the approximate gradients $\frac{\partial F_1}{\partial \beta_{A,B,C}}$ is shown at a particular point in the design space for a complex perturbation of $h = i10^{-15}$. The results are shown for a range of convergence tolerances of the 1D FV solver. It can be noted that the gradients are exact to the accuracy of the function evaluations based on the respective convergence tolerances.

In Table 3 we now compare the complex step gradient of $\frac{\partial F_1}{\partial \beta_A}$ to those obtained using first order accurate forward differencing and second order accurate central differencing for a solver convergence tolerance of 10^{-10}. The results illustrate the unreliability of the differencing methods, particularly with respect to step size. As the step sizes are reduced below 10^{-4} the differencing errors start to dominate and the approximated gradients tend away from the real gradients. The second order central differencing, for a step size of 10^{-4}, is accurate up until the eight decimal place but requires $2N$ function evaluations where as the complex step method requires only N function evaluations.

Table 2: Function gradient with respect to material properties as approximated by the complex step method as a function of the FV solver convergence tolerance.

Convergence tolerance	$\partial F_1/\partial \beta_A$	$\partial F_1/\partial \beta_B$	$\partial F_1/\partial \beta_C$
10^{-4}	-0.25026927	0.07442945	0.19017041
10^{-6}	-0.25024582	0.07440200	0.19015768
10^{-8}	-0.25024616	0.07440078	0.19015755
10^{-10}	-0.25024616	0.07440078	0.19015755

Table 3: Approximated gradient $\partial F_1/\partial \beta$ using finite differencing.

h	Forward Difference	Central Difference
10^{-2}	-0.24900826	-0.25026592
10^{-3}	-0.24978347	-0.25024629
10^{-4}	-0.24805891	-0.25024619
10^{-5}	-0.22972142	-0.25025599
10^{-6}	0.	-0.25031112

complex step approximation (for $h = i10^{-15}$): -0.25024616

For the remainder of the paper, all gradients are computed using the complex step method with a step size of $h = i10^{-15}$.

4 Results

4.1 Test Case 1: invertibility of the problem

As a first test, we investigate the invertibility of the problem for each of the 4 cost functions defined in Section 3.2. We will attempt to recover the design variables for Bifurcation 1 defined in Table 1. The BFGS upper and lower bounds are set to be a factor 10 greater or smaller than the known values used to generate the synthetic data, where the same starting point is used in all test cases. The synthetic data, for both the pressure-time data as well as the Q-time data contain 1000 data points in time.

The converged design variables for the 4 cost functions is shown in Table 4. Both cost function 2 and 3, where respectively Q-time data is included and A_{0_A} is fixed was capable of obtaining the exact design variables (within convergence tolerance). While it is difficult to judge whether the design spaces for F_2 and F_3 are multi-modal, numerical experimentation suggests that they are not. The problem is however ratio based with respect to both β and A_0, where the design space has a very complex valley. It is therefore not too surprising that over 200 BFGS iterations are required to obtain convergence for only 10 and 9 design variables respectively.

Using only pressure-time data as has been demonstrated is ill-posed and therefore the design space is easily shown to be multi-modal. The results in Table 4 confirms this, where F_1 has converged to a local minimum. Including a 'time for arrival' constraint (F_4) does not remove this multi-modality. In order to apply these two cost functions will therefore require either random multi-start (when using gradient based optimisation algorithms) or a global optimiser.

4.2 Test Case 2: Number of data points in time

Using only cost function F_2, we now compare the dependency of the problem to the number of data points (N) contained within both the pressure-time and Q-time signals. The results of the 10 design variables is shown in Table 5 for a range of $N = [20 : 1000]$. It may be noted that there is no observable deterioration of the results for a decreased number of data points. In fact, the problem appears to be

Table 4: Converged design variables for the inverse optimisation formulations.

		Cost Function Formulation			
	Exact	F_1	F_2	F_3	F_4
# BFGS Iterations	-	160	230	223	201
#Func and Grad Eval.	-	193	270	293	370
β_A	113487	102926.5	113488.2	113483.4	109724.0
β_B	226974	205851.0	226973.6	226970.4	219450.4
β_C	453948	411702.3	453909.1	453971.9	438891.1
A_{0_A}	4.0	4.8630862	4.0000796	-	4.2789722
A_{0_B}	0.5	0.6078757	0.4999945	0.5000146	5.3487395
A_{0_C}	3.5	4.2545903	3.4997997	3.5003841	3.7446442
R_{t_B}	0.5	0.50000653	0.4999977	0.49999203	0.5000045
R_{t_C}	0.5	0.5000056	0.5000046	0.5000022	0.4999761
K	1.5×10^4	1.49997×10^4	1.4999×10^4	1.50001×10^4	1.50003×10^4
T	0.3	0.29999997	0.3	0.2999998	0.3000001

Table 5: Comparison of the converged design variables as a function of the number of data points N located within the pressure-time and Q-time signals using cost function F_2.

	Exact	$N = 1000$	$N = 200$	$N = 100$	$N = 50$	$N = 20$
# BFGS Iterations	-	230	331	385	160	176
#Func and Grad Eval.	-	270	370	403	197	241
β_A	113487	113488.2	113490.4	113251.6	113489.5	113487.0
β_B	226974	226973.6	226979.7	226460.5	226977.6	226976.
β_C	453948	453909.1	453955.8	452861.4	4.5393113	453983.2
A_{0_A}	4.0	4.0000796	3.9998163	4.0175384	4.0000034	4.0000481
A_{0_B}	0.5	0.4999945	0.4999732	0.5023955	0.4999873	0.4999893
A_{0_C}	3.5	3.4997997	3.4998280	3.5086637	3.5000985	3.5005494
R_{t_B}	0.5	0.4999977	0.5000019	0.4998767	0.5000085	0.5000066
R_{t_C}	0.5	0.5000046	0.4999972	0.5001626	0.5000070	0.5000195
K	1.5×10^4	1.4999×10^4	1.5000×10^4	1.4997×10^4	1.5000×10^4	1.4999×10^4
T	0.3	0.3	0.3	0.299997	0.3	0.3

better behaved for fewer data points. These results however should be viewed with some caution. The synthetic time signals are for a single bifurcating artery which are fairly simple time signals. Should the complexity of the network be increased the resulting time signals' complexity will also increase, in which case more data points might be necessary.

4.3 Test Case 3: Addition of random noise

The last problem we investigate is the invertibility of the problem for increasing levels of noise in the synthetic data. The random noise is added point for point such that:

$$\begin{aligned} P(t_i) &= P(t_i) + R_{i_1} P_{\max}, \quad \text{for } i = 1, .., N \\ Q(t_i) &= Q(t_i) + R_{i_2} Q_{\max}, \quad \text{for } i = 1, .., N \end{aligned} \tag{23}$$

where R_{i_1} and R_{i_2} is a different uniform random number for each data point between 0 and 1. Subscripts $\cdot_{\max}$ refer to the maximum value in the P and Q time signals.

Table 6 show the results using the cost function F_2 for added noise levels of 1%, 5% and 10% of the magnitude of the signals with $N = 1000$. The invertibility of the branching vascular problem is highly dependant on the added noise. Noise levels of 10% leads to converged design variables that differ in many instances by more than a factor two from the expected quantities.

Table 6: Comparison of the converged design variables as a function of the level of noise within the pressure-time and Q-time signals using cost function F_2.

	Exact	No Noise	1% Noise	5% Noise	10% Noise
# BFGS Iterations	-	230	215	112	103
#Func and Grad Eval.	-	270	256	130	124
β_A	113487	113488.2	120712.26	171451.7	226974.0
β_B	226974	226973.6	227281.0	228564.2	214775.9
β_C	453948	453909.1	425771.7	324143.3	297761.7
A_{0_A}	4.0	4.0000796	4.0364606	4.3439269	4.1243062
A_{0_B}	0.5	0.4999945	0.5029177	0.5188061	0.6673710
A_{0_C}	3.5	3.4997997	3.6517644	4.1530419	4.3944750
R_{t_B}	0.5	0.4999977	0.49711447	0.4807226	0.39750310
R_{t_C}	0.5	0.5000046	0.52435923	0.6087471	0.7027408
K	1.5×10^4	1.4999×10^4	1.5216×10^4	1.6271×10^4	1.7853×10^4
T	0.3	0.3	0.300219	0.301145	0.299832

5 Concluding remarks and future work

In this paper we investigated the invertibility of a single bifurcating artery where a uniform β and A_0 for each of the vessels in a bifurcation were defined as design variables along with variables characterising both the input and output boundary conditions. We demonstrated, given a pressure-time signal at a single location, in addition to either the Q-time signal at the same location or fixing a single vessel A_0 parameter leads to a uniquely invertable problem. There appears to be little dependence on the number of data points located within these time signals. However the signals must be fairly accurate, where the measurement noise levels should not be much higher than a few percent.

Future work will focus on extending the inverse analysis to a larger vascular network.

6 References

[1] A.E.J. Bogaers, A.M. de Villiers, S. Kok, O. Ubbink, T. Franz, B.D. Reddy, and C.G. du Toit. Towards the development of a fully coupled arterial-venous 1d model. *10th World Congress on Computational Mechanics, São Paulo, Brazil*, 2012.

[2] J. Degroote, I. Couckuyt, J. Vierendeels, P. Segers, and T. Dhaene. Inverse modelling of an aneurysm's stiffness using surrogate-based optimization and fluid-structure interaction simulations. *Structural and Multidisciplinary Optimization*, 2011.

[3] V. Martin, F. Clément, A. Decoene, and J.F. Gerbeau. Parameter identification for a one-dimensional blood flow model. In *ESAIM: Proceedings*, volume 14, pages 174–200, 2005.

[4] J. Martins, P. Sturdza, and J. Alonso. The complex-step derivative approximation. *ACM Trans. Math. Softw.*, 29(3):245–262, 2003.

[5] J. P. Mynard and P. Nithiarasu. A 1d arterial blood flow model incorporating ventricular pressure, aortic valve and regional coronary flow using the locally conservative galerkin (lcg) method. *Communications in Numerical Methods in Engineering*, 24:367–417, 2008.

[6] A. Quarteroni and L. Formaggia. Mathematical modelling and numerical simulation of the cardiovascular system. *Handbook of numerical analysis*, 12:3–127, 2004.

[7] Ciyou Zhu, Richard H. Byrd, Peihuang Lu, and Jorge Nocedal. Algorithm 778: L-bfgs-b: Fortran subroutines for large-scale bound-constrained optimization. *ACM Trans. Math. Softw.*, 23(4):550–560, December 1997.